Available online at www.sciencedirect.com
SCIENCE DIRECT®
Journal of Power Sources 139 (2005) 242–249
JOURNAL OF POWER SOURCES
www.elsevier.com/locate/jpowsour

Pyrolysis of hexa(phenyl)benzene derivatives: a molecular approach toward carbonaceous materials for Li-ion storage

Thierry Renouard[a], Lileta Gherghel[b], Mario Wachtler[c,1], Franco Bonino[c,**], Bruno Scrosati[c], Richard Nuffer[a], Claude Mathis[a,*], Klaus Müllen[b,**]

[a] *Institut Charles Sadron UPR 22 (CNRS), 6 rue Boussingault, 67083 Strasbourg Cedex, France*
[b] *Max-Planck Institute for Polymer Research, Ackermannweg 10, 55124 Mainz, Germany*
[c] *University of Rome "La Sapienza", Piazzale Aldo Moro 5, 00185 Roma, Italy*

Received 14 May 2004; accepted 22 June 2004
Available online 11 September 2004

Abstract

Hexa(phenyl)benzene (HPB) and hexakis(*p*-bromophenyl)benzene (HPB-Br) were submitted to controlled pyrolysis under mild conditions to prepare carbonaceous materials for Li-ion storage. Experiments were performed in evacuated sealed ampoules and different temperatures (in the range 500–600 °C) and heating times (1 upto 5 days) were applied. Pyrolytic products were obtained as black flakes and characterised by elemental analysis, thermogravimetric analysis, UV–vis–NIR and Raman spectroscopies. Scanning electron microscopy exhibited several structures (nanorods, bundles, microspheres) on the surface of the flakes, depending on the precursor and on the pyrolysis procedure. Preliminary electrochemical measurements revealed lithium storage capacities upto 500 mAh g^{-1}.
© 2004 Elsevier B.V. All rights reserved.

Keywords: Lithium-ion; Graphitic carbon; Pyrolysis; Scanning electron microscopy

1. Introduction

There has been a keen interest in rechargeable lithium-ion batteries since the commercialisation of the first cell by Sony in the early 90s. The primary advantages of Li-ion technology include high potential, small size and low weight that afford gravimetric energy densities higher than 130 Wh kg^{-1} for a lifespan exceeding 1000 cycles [1–5]. Consequently, Li-ion batteries find applications in numerous portable devices (e.g. cellular phone, lap-top computer, camcorder) and they are expected to be a major breakthrough for electric vehicles. Though the Li-ion battery market matures, a great deal of R&D effort is still needed to face ongoing mobile equipment innovations. Therefore, extensive research activity is devoted to further improve the performance of the three components of these batteries, i.e. the cathode, the electrolyte and the anode. Solid-state chemists are deeply involved in the development of lithium transition metal oxides [6–10] since these reversible lithium intercalation hosts successfully operate as cathodes in Li cells. Current trends in the field of electrolytes tend to replace the conventional liquid electrolyte with lithium-conducting polymer electrolytes [11–15]. In the case of anodes, widespread carbon-based feedstocks are commonly recognised as some of the best materials. This choice is governed by their lightness associated to their ability to reversibly incorporate guest molecules such as alkali metal ions. Presently, graphite is largely used in commercial cells but its lithium storage capacity is limited to 372 mAh g^{-1}, corresponding to the LiC_6 stage.

In the search for more efficient anodic materials, we propose a new concept to reach three-dimensional graphitic arrangements as follows: (i) to start at a molecular level

* Corresponding author. Tel.: +33 3 8841 4156; fax: +33 3 8841 4099.
** Co-corresponding author.
E-mail address: cmathis@ics.u-strasbg.fr (C. Mathis).
[1] Present address: Center for Solar Energy and Hydrogen Research, Helmholtzstrasse 8, 89081 Ulm, Germany.

0378-7753/$ – see front matter © 2004 Elsevier B.V. All rights reserved.
doi:10.1016/j.jpowsour.2004.06.069

from carbon-rich, benzene-based precursors and (ii) to induce intermolecular aryl–aryl couplings and simultaneous or subsequent intramolecular dehydrogenation to obtain graphene disks being part of a 3D-network. Recently, nano-sized propeller-shaped graphitic molecules were obtained by metal-catalysed cyclodehydrogenation of three-dimensional dendritic oligophenylenes [16]. It has already been observed that heat treatment of poly(*p*-phenylenes) also results in the formation of planar graphene units by thermal hydrogen elimination combined with fusion of benzene rings [17]. Moreover, a convenient way has been developed to prepare carbon nano- and micro-particles by pyrolysis of well-defined polycyclic aromatic hydrocarbons (PAHs) under mild conditions [18]. Thus, we assumed that by carefully tailoring the pyrolysis procedure, both crosslinking of oligophenylenes and thermal cyclodehydrogenation might be feasible in the same reactor. Hexa(phenyl)benzene (HPB) and hexakis(*p*-bromophenyl)benzene (HPB-Br) were selected as starting materials, since they can be considered as the smallest branched 3D-oligophenylenes. The synthesis, characterisation and preliminary results of lithium storage capacities of a set of pyrolysed materials are reported in this work.

2. Experimental

2.1. General

Elemental analysis was run on a CHNS Microanalyser EA1112 from ThermoFinnigan. A LEO 1450VP Oxford Instrument and a LEO 1530 field emission scanning electron microscope were used for SEM investigations. TGA spectra were measured on a Mettler TG 50 Thermobalance. The optical absorption measurements were performed at ambient temperature on a UV–vis–NIR Perkin-Elmer Lambda 900 spectrometer. Raman spectra were measured as KBr pellets and recorded on a Dilor XY 800 spectrometer with a liquid-nitrogen cooled CCD detector and Raman microscopical unit. An Ar+ laser (514.5 nm) was used as excitation source. Cyclic voltammetric measurements (CV) were carried out using a 213 Par potentiostat coupled with a software especially developed in our laboratories. A Maccor battery cycling was used for galvanostatic cycling (GC).

2.2. Synthesis of precursors

The synthesis of HPB is well-established and allows its preparation on a large scale [19]. Starting from tetraphenylcyclopentadienone, diphenylacetylene and diphenylether (as solvent) HPB was obtained via a Diels–Alder cycloaddition that releases only carbon monoxide. An original method for bromination of HPB has been developed by Rathore et al. which consists in a simple stirring with neat bromine in chilled ethanol [20]. A comparable route was applied but without any solvent, so post-treatment was reduced to elimination of bromine excess. Purification was performed by filtering a hot THF solution of the product, which allowed to remove the residual inorganic salts. The ^{1}H and ^{13}C NMR data were in agreement with a hexa-brominated compound. No evidence of less halogenated derivatives was observed.

2.3. Pyrolysis

Experiments were carried out in evacuated (10^{-5} mbar), sealed quartz or glass ampoules in an electrical oven. The pyrolysis programs allowed: (i) slow heating (12 h) to the desired temperature; (ii) pyrolysis for different times; and (iii) cooling down to room temperature in 12 h (vide infra). The products were removed from the walls of the ampoules, extracted with refluxing THF to eliminate the soluble parts and dried under reduced pressure (10^{-3} mbar). These experiments were performed on a gram scale and were well reproducible.

2.4. Electrochemical measurements

The electrochemical experiments were carried out using two- and three- electrode cells. The reference and counter electrodes were metallic Li disks of 10 mm diameter. The working electrodes for galvanostatic cycles were prepared as follows: first, active materials and small quantities of poly(vinylidene difluoride) (PVdF) were mixed. PVdF was used as a binder to ensure a good mechanical stability of the electrode films. When necessary, a better electronic contact throughout the film was obtained by adding 14% of an electronic carbon conductor (extremely fine powder Super P). This mixture was then dispersed in a suitable solvent (usually *N*-methyl pyrrolidinone) and stirred for several hours. The final active materials preparation was poured on a thin copper foil and spread by sliding a stainless steel blade (Doctor Blade) all over the length of the foil. The film thickness (normally 0.1 mm) was set by adjusting the distance of the blade from the copper foil. After evaporation of the solvent, the thin electrode film obtained was cut as small disks of 10 mm diameter and dried at 120 °C under vacuum to eliminate the residual solvent and humidity. The electrodes for CV experiments were prepared using the same technique but without addition of Super P. The electrolyte was a 1 M solution of $LiClO_4$ in EC:DEC (ethyl carbonate:diethyl carbonate) or EC:DMC (ethyl carbonate:dimethyl carbonate) 1:1 molar ratio. All cells were assembled in a MBraun dry box, under an argon atmosphere and a water content below 1 ppm. All galvanostatic cycles were carried out at a current rate of C/5, which represents the current necessary to discharge the active electrode materials in 5 h. The actual current density was calculated using the maximum capacity of graphite (372 mAh g^{-1}).

Table 1
Detailed experimental conditions for pyrolysis of HPB in quartz ampoules

Sample	Temperature (°C)	Time (h)	Elemental analysis (%)
HPB	–	–	93.79 (C); 5.97 (H)
1	600	24	94.04 (C); 2.82 (H)
2	600	60	96.45 (C); 2.66 (H)
3	600	108	98.93 (C); 1.03 (H)

3. Results and discussions

3.1. Pyrolysed materials

3.1.1. Pyrolysis of hexa(phenyl)benzene (HPB)

The pyrolysis of HPB at 600 °C in quartz ampoules led to the formation of different pyrolytic products, depending on the duration of the heating (Table 1). Heat treatment for 24 h produced a mixture of dark brown soluble and insoluble materials (sample 1). In comparison to the starting product, elemental analysis of the pyrolytic compound showed an increase of the carbon–hydrogen ratio. This material was investigated by UV–vis spectroscopy and scanning electron microscopy. The UV–vis spectrum of the soluble part of the sample showed an intense absorption band at 320 nm, which is red shifted compared to the absorption band of the starting compound (290 nm) (Fig. 1). A similar spectrum was observed in the case of $C_{30}H_{16}$, an all-benzenoid polycyclic aromatic hydrocarbon (PAH) containing five so-called "full" aromatic rings (fused benzene rings), synthesised by oxidative cyclodehydrogenation [16,21–23]. Additionally, several shoulders were detected between 360 nm and 500 nm. They can be attributed to larger all-benzenoid PAHs containing between 6 and 10 "full" fused benzene rings, based upon a comparison with the UV–vis spectra of authentic PAHs obtained by direct chemical synthesis [16,21–23].

Raman spectroscopy gave significant information about the extension of the π-conjugation. Thus, the first-order Raman spectrum of sample 3 (washed and dried) exhibited only two bands, one at 1334 cm^{-1} with a shoulder at 1260 cm^{-1} and a second one at 1600 cm^{-1} (Fig. 2). The positions and relative intensities of the bands were similar to those of large all-benzenoid polycyclic aromatic hydrocarbons with 10–22 "full" fused benzene rings recorded under identical conditions [24–30].

Combining the results from UV–vis and Raman spectroscopies suggests the formation of all-benzenoid PAHs as a consequence of thermal cyclodehydrogenation processes and supports the anticipated mechanism with intermolecular crosslinking and fusion of the benzene rings during heat treatment at 600 °C. After pyrolysis for 24 h, PAHs with a minimum of five "full" fused benzene rings could be already detected. Prolonged pyrolysis for 60 and 108 h, respectively, led to a gradual increase in the size of the obtained PAHs, as revealed by elemental analysis.

Scanning electron microscopy of the insoluble parts of sample 1 (obtained after washing with THF, filtration and drying under reduced pressure) showed that the top of the film was partially coated by discrete microobjects with different forms and dimensions (Fig. 3a). After 60 h pyrolysis (sample 2), the shape of these objects became more uniform and short rods were the major structures seen in the SEM images (Fig. 3b). The outer diameters of these structures were about 100 nm and the lengths were upto 1 μm. The product obtained after prolonged pyrolysis for 108 h (sample 3) was black and almost insoluble in organic solvents. Elemental analysis showed that more than 35 % of the original hydrogen content had been removed. The morphology of the obtained compound was probed by SEM. The more or less isolated nanorods, detected on the top of the film after pyrolysis for 60 h now became even longer and formed bundles of thin, elongated fibrils with diameters of about 100 nm and lengths upto 5 μm. Furthermore, these bundles formed extended, porous networks and covered the surface of the film (Fig. 3c). In some areas, spherical particles with diameters ranging from a few hundred nanometers to 4 μm were also seen, which were comparable to the radial spherical textures obtained by pyrolysis of hexa(alkyl)substituted hexa-peri-hexabenzocoronene [18] and during carbonisation of a variety of carbonaceous precursors [31,32]. The spherical objects were often coated by the network of the long fibrils (Fig. 3d).

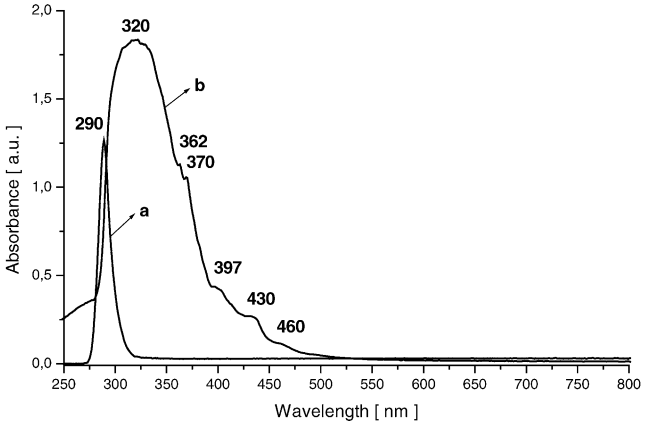

Fig. 1. UV–vis spectra of HPB (a) and of the soluble part of sample 1 (b).

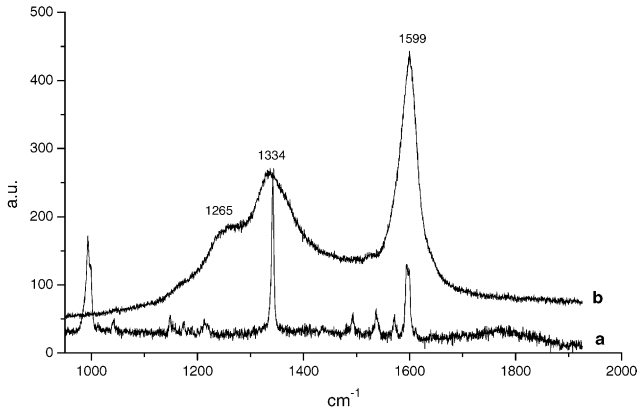

Fig. 2. Raman spectra of HPB (a) and of sample 3 (b).

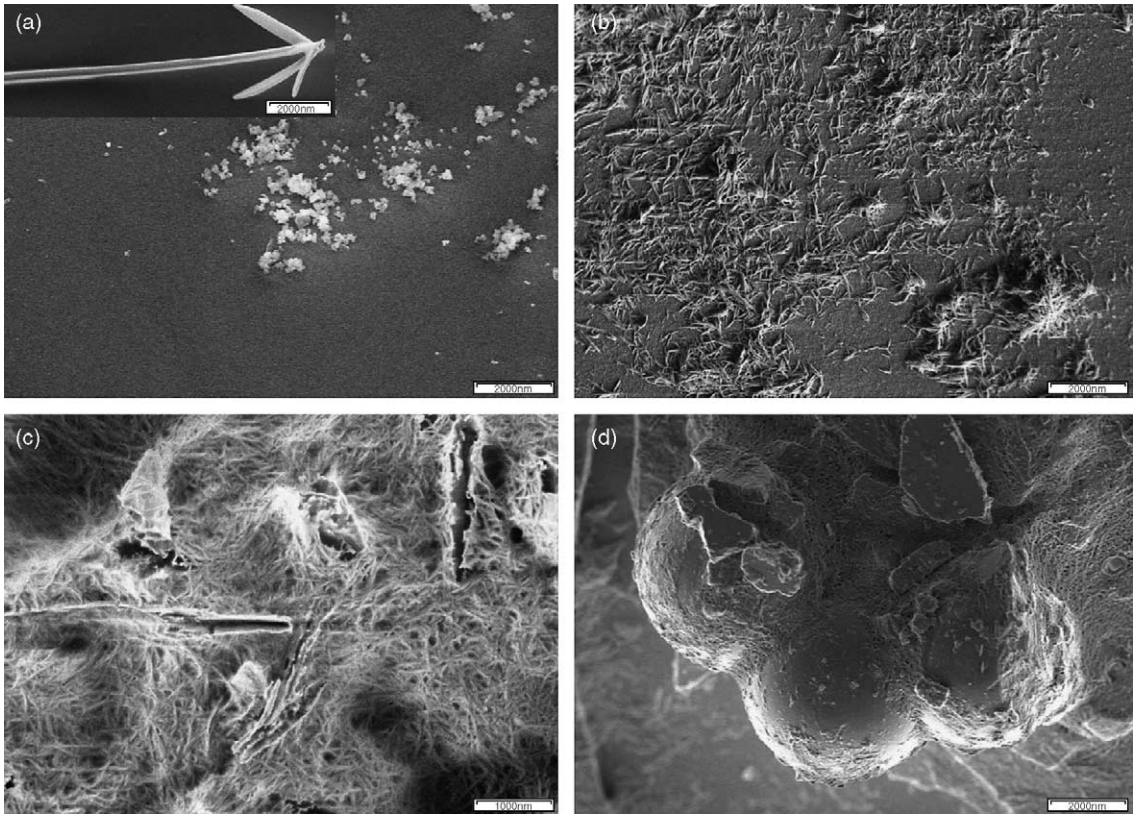

Fig. 3. SEM micrographs of the products obtained by pyrolysis of HPB at 600 °C: after 24 h (a and inset), after 60 h (b) and after 108 h (c and d); Scale bars: (c) 1 μm, (a, inset, b and d) 2 μm.

Table 2
Detailed experimental conditions for pyrolysis of HPB-Br in glass ampoules

Sample	Temperature (°C)	Time (h)	Soluble part	Elemental analysis (%)
HPB-Br	–	–	–	50.07 (C); 2.55 (H); 46.6 (Br)
4	600	24	Traces	84.48 (C); 1.49 (H); 3.54 (Br)
5	580	72	5%	91.23 (C); 1.64 (H); 2.36 (Br)
6	550	72	8%	93.04 (C); 1.95 (H); 2.38 (Br)
7	500	120	10%	95.38 (C); 2.14 (H); 1.06 (Br)

The influence of prolonged cooling process (for 36 h) on the morphology of the pyrolytic compound was investigated but no significant effect was observed on the final products.

3.1.2. Pyrolysis of hexakis(p-bromophenyl)benzene (HPB-Br)

For HPB-Br as a pyrolysis precursor, different temperatures and heating times were tested in evacuated sealed glass ampoules (Table 2)[1]. Since bromine atoms are better leaving groups than hydrogens, they were assumed to facilitate the intermolecular aryl–aryl couplings, and so the formation of large branched 3D-polyphenylenes at lower temperatures. As for HPB, the black products obtained from HPB-Br were recovered as films coating the glass walls. All thin films were insoluble in common organic solvents and evaporation of the washings (see Section 2) revealed only limited amounts of soluble parts. Thermogravimetric analysis showed that the products were extremely thermally stable over a wide range of temperatures (upto 900 °C) under inert atmosphere. Around 5% weight loss was usually observed, which can be related to gradual evaporation of insoluble small molar mass compounds trapped within the intercalation structures. No thermal oxidation of the products occurred before 450 °C under air. Although the materials formation was assumed to proceed by radical couplings, no ESR signal could be detected for the final compounds. Elemental analyses revealed that the higher the temperature of pyrolysis the lower the remaining hydrogen content, regardless of the heating time. Conversely, decreasing the pyrolysis time resulted in larger bromine contents (i.e. less crosslinked structures), although higher temperatures were applied. Indeed, pyrolysis for 5

[1] Note that for batches at 600 °C heating was always stopped after 24 h since the glass ampoules started to expand.

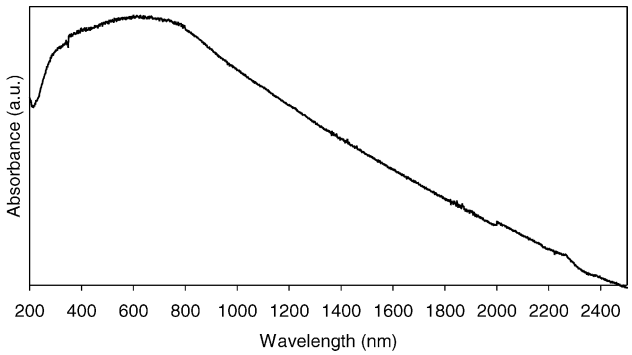

Fig. 4. Solid-state UV–vis–NIR spectrum of sample 6.

days at 500 °C produced materials containing 1.06% of residual Br, while pyrolysis for one day at 600 °C still gave 3.54% of Br. Bromine doping of graphite has been known for long [33–35]. In that case, bromine is present in the interlayer space between graphite sheets in the form of Br_2-molecules. Since our materials still contain hydrogens that can further react with Br_2, the remaining bromine content is assumed to correspond to bromine atoms bound to carbons. Furthermore, it has been shown by Nishikawa et al. that bromine doping of artificial graphite obtained at relatively low temperatures led to formation of C–Br bonds by reaction of Br_2 with dandling bonds of carbon [36]. Even though all the products were insoluble, UV–vis–NIR spectra were measured on a quartz plate coated by thin films obtained by spray deposition of finely powdered materials dispersed in methanol. The UV–vis–Nir spectrum of sample 6 is depicted in Fig. 4. Due to the broad bands, no typical absorption wavelength can be distinguished. Nevertheless, since the absorption covers the entire visible range and based upon comparison with previously reported PAHs [16,21–23], one can estimate that the materials are composed of large graphene units incorporating upto 35–40 fused aromatic rings. The reported elemental analysis is in accordance with such extended structures. All these data confirm the interest of the brominated derivative of HPB. Indeed, by applying mild pyrolysis conditions (550 °C for 3 days) the materials obtained exhibit higher graphitisation rate as compared with HPB-based materials prepared from pyrolysis at 600 °C for almost 5 days and the crude product contains very low amounts of soluble fraction. Moreover, the fact that the pyrolysis temperature is reduced to 550 °C is of practical importance since then glass ampoules can be used.

As previously observed for HPB-based materials, both sides of the films exhibit a different appearance. Whereas the external face (in contact with the glass walls) of the foil was smooth with metallic brightness, the internal face was dull. SEM images revealed that the internal face was coated by layers of microspheres (Fig. 5) that closely resemble the so-called “mesocarbon microbeads” (MCMBs) [37]. Intriguingly, the dimensions of the beads (Fig. 5a) were relatively homogeneous, since most of the diameters were in the range 5–7 μm. As displayed by the edge plane image, the beads are fused to one another. Since these beads are present only on the surface facing the internal part of the ampoules, one can assume this difference of texture to be due to the lack of material able to sublime at the final stage of the pyrolysis. This is emphasised by the low ratio of the layer thickness of beads compared to the thickness of carbon bulk.

3.2. Electrochemical measurements

Preliminary CV experiments were performed using samples 3 and 5 (Fig. 6). Although the pyrolysis conditions were quite similar, the electrochemical behaviour of the samples clearly depends on the final product, i.e. on the starting material used. CV cycles of sample 3 (carried out at 0.2 mV s^{-1}) are reported in Fig. 6a. The cathodic current at the low limit potential (near 0 V versus Li) is related to Li insertion into the carbon host, while the cathodic peaks in the range 200–250 mV can be assigned to both reversible and irreversible processes, these latter being attributed to the formation of a protective, passivation layer on the electrode surface [1]. The anodic peaks at 300 mV versus Li represent the Li deinsertion process from the host material. Both anodic and cathodic peaks are very sharp, which is related to the surface area characteristics and is generally observed with pure phase materials. The reported values are in accordance with typical redox potential ranges of natural carbons. CV cycles of sample 5 are shown in Fig. 6b, using the same experimental conditions as for sample 3. The cathodic and anodic

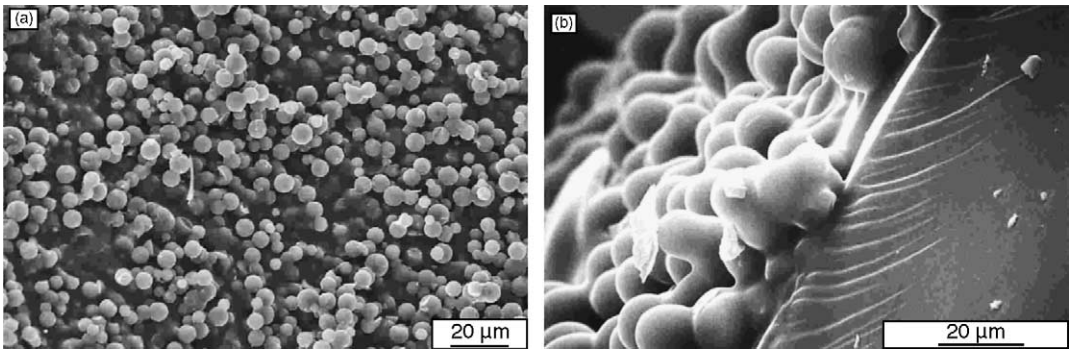

Fig. 5. SEM micrographs of sample 5. Internal face (a) and edge plane (b).

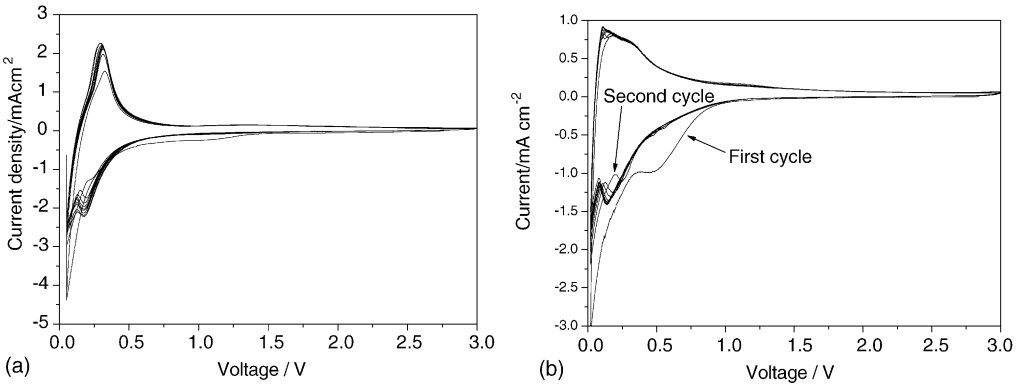

Fig. 6. CV at 0.2 mV s^{-1} of sample 3 (a) and sample 5 (b).

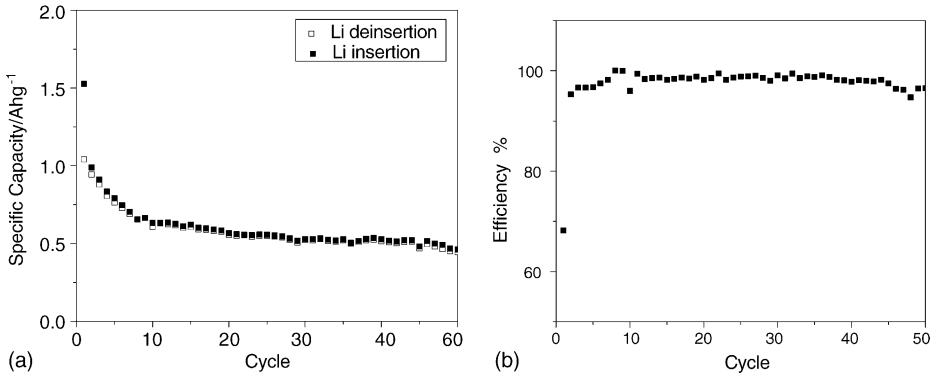

Fig. 7. Specific capacity during galvanostatic cycles at C/5 of sample 3 (a). Efficiency of the Li insertion/deinsertion process over the first 50 galvanostatic cycles at C/5 (b).

peaks appear at similar potentials than for sample 3, but they exhibit different shapes since at least two cathodic and two anodic peaks can be distinguished. Another major difference between the CV of the two samples is noteworthy during the first cycle: for sample 3, only a small increase of current starting from 1250 mV versus Li can be detected, while for sample 5 an important cathodic peak at 500 mV versus Li appears. In both cases, minor evolutions can also be seen between the second and the following cycles. Many different parameters can be responsible for these variations [40], the most likely being irreversible reactions taking place at the electrode/electrolyte interface. Description and analysis of all the parameters are outside the scope of this preliminary report, but further work in this direction is under progress.

Fig. 7a shows the specific capacities of lithium storage delivered during the first 50 Li insertion/deinsertion galvanostatic (C/5) cycles for sample 3. After some capacity fading, the values stabilise around 500 mAh g^{-1}, i.e. much higher

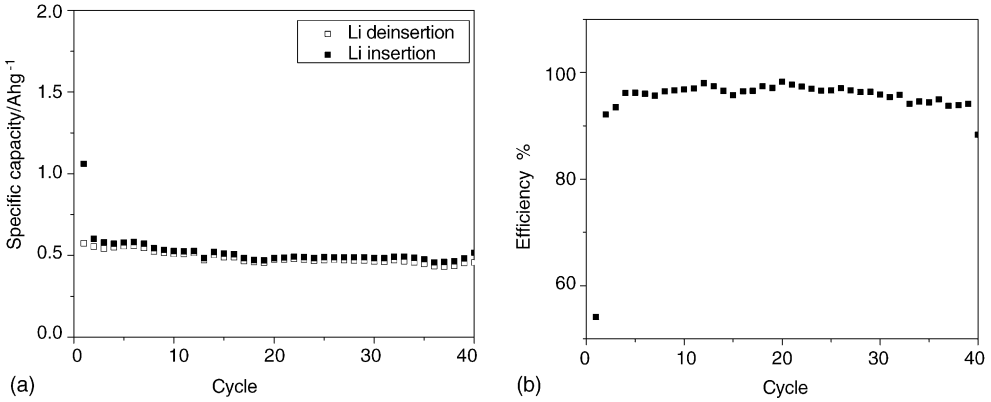

Fig. 8. Specific capacity during galvanostatic cycles at C/5 of sample 5 (a). Efficiency of the Li insertion/deinsertion process over the first 40 galvanostatic cycles at C/5 (b).

than the maximum value for pure graphite (372 mAh g^{-1}). The efficiency of the Li insertion/deinsertion processes reaches 99% after 7 cycles (Fig. 7b). This behaviour is in agreement with CV data: as Fig. 6a shows, no important irreversible cathodic peak is present during the first cycle and one may assume that irreversible reactions are displaced not only on the first cycle, but rather over several subsequent cycles, this in turn lowers the corresponding efficiency.

The behaviour of sample 5 is different. Fig. 8a shows the specific capacity of lithium storage delivered during the first 40 Li insertion/deinsertion galvanostatic (C/5) cycles for sample 5. Specific capacity data in both Figs. 7 and 8 are based on the actual active electrode mass and the error on the active mass weight is about 8%. Even though some capacity fading is observed in the early beginning, the values rapidly stabilise around 500 mAh g^{-1}. In agreement with the CV results, a high irreversible capacity is observed only during the initial cycle indicating that the protective layer is mainly produced during this first cycle. This can lead to a non-optimised protective layer that in turn can lower the efficiency during the following cycles, i.e. around 95–97% (Fig. 8b). All these preliminary results were obtained using limited amounts of pristine materials and, we may anticipate that optimisation of the electrode morphology (e.g. control of the particle size) should give rise to a significant increase of both the specific capacity and the efficiency [41].

4. Conclusions

The work described here shows the unique combination of: (i) the preparation of promising materials for Li-ion storage by pyrolysis of carbon-rich, benzene-based precursors and (ii) the possibility to easily upscale the stepwise method established. Furthermore, our materials, when assembled as electrodes in a lithium cell, revealed a specific capacity almost doubled compared to pure graphite. Many carbon materials have been tested since Li-ion cells research began in 1985 [42,43]. Many of them show very high specific capacitiy, but at present the graphitic materials seem to be the best choice. This is due to some carbon problems such as the high value of irreversible capacity and a rapid decrease of the reversible capacity during cycling. The materials here presented show interesting capacity values after 50 cycles, but they need further optimisation of the pyrolysis conditions as well as a better comprehension of the electrochemical reactions to allow the production of efficient materials for advanced Li-ion batteries. Indeed we expect to reach specific capacities exceeding 600 mAhg^{-1} for hundreds of cycles.

Acknowledgements

This work was performed by the financial support of the European Community (RTD program: GRD-CT-2001-00571). Special thanks to R. Roth (ICS, elemental analysis of Br), S. Natale (University of Rome, electrode preparation), H.-J. Menges (MPI-P, Raman spectroscopy) and G. Glasser (MPI-P, SEM measurements).

References

[1] M. Wakihara, O. Yamamoto (Eds.), Lithium-Ion Batteries: Fundamentals and Performance, Wiley VCH, Weinheim, 1998, pp. 1–247.
[2] W.A. van Schalkwijk, B. Scrosati (Eds.), Advances in Lithium-Ion Batteries, Kluwev Academic, 2002, pp. 1–513.
[3] J.M. Tarascon, M. Armand, Issues and challenges facing rechargeable lithium batteries, Nature 414 (6861) (2001) 359–367.
[4] B.A. Johnson, R.E. White, Characterization of commercially available lithium-ion batteries, J. Power Sources 70 (1) (1998) 48–54.
[5] P.G. Bruce, Solid-state chemistry of lithium power sources, Chem. Commun. (1997) 1817–1824.
[6] K. Ozawa, Lithium-ion rechargeable batteries with $LiCoO_2$ and carbon electrodes: the $LiCoO_2$/C system, Solid State Ionics 69 (3–4) (1994) 212–221.
[7] Jones CDW, E. Rossen, J.R. Dahn, Structure and electrochemistry of $Li_xCr_yCo_{1-y}O_2$, Solid State Ionics 68 (1–2) (1994) 57–63.
[8] R. Stoyanova, E. Zhecheva, L. Zarkova, Effect of Mn-substitution for Co on the crystal structure and acid delithiation of $LiMn_yCo_{1-y}O_2$ solid solutions, Solid State Ionics 73 (3–4) (1994) 233–240.
[9] M. Holzapfel, R. Schreiner, A. Ott, Lithium-ion conductors of the system $LiCo_{1-x}Fe_xO_2$: a first electrochemical investigation, Electrochim. Acta 46 (7) (2001) 1063–1070.
[10] C. Delmas, I. Saadoune, A. Rougier, The cycling properties of the $Li_xNi_{1-y}Co_yO_2$ electrode, J. Power Sources 44 (1–3) (1993) 595–602.
[11] B. Scrosati, C.A. Vincent, Polymer electrolytes: the key to lithium polymer batteries, Bull. Mater. Res. Soc. 25 (3) (2000) 28–30.
[12] S. Megahed, B. Scrosati, Rechargeable non-aqueous batteries. The role of lithium systems, Electrochem. Soc. Interface 4 (4) (1995) 34–37.
[13] Q. Shi, M. Yu, X. Zhou, Y. Yan, C. Wan, Structure and performance of porous polymer electrolytes based on P(VDF-HFP) for lithium-ion batteries, J. Power Sources 103 (2) (2002) 286–292.
[14] B.B. Owens, W.H. Smyrl, J.J. Xu, R&D on lithium batteries in the USA: high-energy electrode materials, J. Power Sources 81–82 (1999) 150–155.
[15] J.M. Tarascon, A.S. Gozdz, C. Schmutz, F. Shokoohi, P.C. Warren, Performance of Bellcore's plastic rechargeable Li-ion batteries, Solid State Ionics 86–88 (1996) 49–54.
[16] C.D. Simpson, G. Mattersteig, K. Martin, L. Gherghel, R.E. Bauer, H.J. Räder, K. Müllen, Nanosized molecular propellers by cyclodehydrogenation of polyphenylene dendrimers, J. Am. Chem. Soc. 126 (10) (2004) 3139–3147.
[17] P. Kovacic, A. Kyriakis, Polymerization of benzene to *p*-polyphenyl by aluminium chloride–cupric chloride, J. Am. Chem. Soc. 85 (4) (1963) 454–458.
[18] L. Gherghel, C. Kübel, G. Lieser, H.J. Räder, K. Müllen, Pyrolysis in the mesophase: a chemist's approach toward preparing carbon nano- and microparticles, J. Am. Chem. Soc. 124 (44) (2002) 13130–13138.
[19] G.R. Newkome, N.B. Islam, J.M. Robinson, Chemistry of heterocyclic compounds. 21. Synthesis of Hexa(2-pyridyl)benzene and the related Phenyl(2-pyridyl)benzenes. Characterization of corresponding substituted cyclopentenolone intermediates, J. Org. Chem. 40 (24) (1975) 3514–3518.

[20] R. Rathore, C.L. Burns, M.I. Deselnicu, Multiple-electron transfer in a single step. Design and synthesis of highly charged cation-radical salts, Org. Lett. 3 (18) (2001) 2887–2890.
[21] M.D. Watson, A. Fechtenkötter, K. Müllen, Big is beautiful-"aromaticity" revisited from the viewpoint of macromolecular and supramolecular benzene chemistry, Chem. Rev. 101 (5) (2001) 1267–1300.
[22] C.D. Simpson, J.D. Brand, A.J. Berresheim, L. Przybilla, H.J. Räder, K. Müllen, Synthesis of a giant 222 carbon graphite sheet, Chem. Eur. J. 8 (6) (2002) 1424–1429.
[23] F. Dötz, J.D. Brand, S. Ito, L. Gherghel, K. Müllen, Synthesis of large polycyclic aromatic hydrocarbons: variation of size and periphery, J. Am. Chem. Soc. 122 (32) (2000) 7707–7717.
[24] F. Negri, C. Castiglioni, M. Tommasini, G. Zerbi, A computational study of the Raman spectra of large polycyclic aromatic hydrocarbons: toward molecularly defined subunits of graphite, J. Phys. Chem. A. 106 (14) (2002) 3306–3317.
[25] C. Mapelli, C. Castiglioni, G. Zerbi, K. Müllen, Common force field for graphite and polycyclic aromatic hydrocarbons, Phys. Rev. B 60 (18) (1999) 12710–12725.
[26] C. Mapelli, C. Castiglioni, E. Meroni, G. Zerbi, Graphite and graphitic compounds: vibrational spectra from oligomers to real materials, J. Mol. Struct. 481 (1999) 615–620.
[27] C. Castiglioni, F. Negri, M. Rigolio, G. Zerbi, Raman activation in disordered graphites of the A_1' symmetry forbidden $k \neq 0$ phonon: the origin of the D line, J. Chem. Phys. 115 (8) (2001) 3769–3778.
[28] C. Castiglioni, C. Mapelli, F. Negri, G. Zerbi, Origin of the D line in the Raman spectrum of graphite: a study based on Raman frequencies and intensities of polycyclic aromatic hydrocarbon molecules, J. Chem. Phys. 114 (2) (2001) 963–974.
[29] M. Rigolio, C. Castiglioni, G. Zerbi, F. Negri, Density functional theory prediction of the vibrational spectra of polycyclic aromatic hydrocarbons: effect of molecular symmetry and size on Raman intensities, J. Mol. Struct. 563 (2001) 79–87.
[30] J. Wu, L. Gherghel, M.D. Watson, J. Li, Z. Wang, C.D. Simpson, U. Kolb, K. Müllen, From branched polyphenylenes to graphite ribbons, Macromolecules 36 (19) (2003) 7082–7089.
[31] A. Oberlin, Carbonization and Graphitization, Carbon 22 (6) (1984) 521–541.
[32] E.J. Roche, Electron-microscopy study of mesophase pitch-based graphite fibers, J. Mater. Sci. 25 (4) (1990) 2149–2158.
[33] W. Rudorff, The solution of bromine in the crystal lattice of graphite: bromine graphite, Z. Anorg. Allg. Chem. 245 (1941) 383–390.
[34] G. Hennig, The properties of intersticial compounds of graphite III. The electrical properties of halogen compounds of graphite, J. Chem. Phys. 20 (9) (1952) 1443–1447.
[35] T. Sasa, Y. Takahasi, T. Mukaibo, Crystal structure of graphite bromine lamella compounds, Carbon 9 (4) (1971) 407–416.
[36] H. Yoshikawa, K. Fukuyama, Y. Nakahara, T. Konishi, N. Ichikuni, Y. Yoshikawa, N. Akuzawa, Y. Takahashi, K. Nishikawa, X-ray absorption fine structure study on residue bromine in carbons with different degrees of graphitization, Carbon 41 (15) (2003) 2931–2938.
[37] O.J. Kwon, Y.S. Jung, J.H. Kim, S.M. Oh, A simple preparation method for spherical carbons and their anodic performance in lithium secondary batteries, J. Power Sources 125 (2) (2004) 221–227.
[40] B. Markovsky, A. Rodkin, Y.S. Cohen, O. Palchik, E. Levi, D. Aurbach, H.J. Kim, M. Schmidt, The study of capacity fading processes of Li-ion batteries: major factors that play a role, J. Power Sources 119–121 (2003) 504–510.
[41] F. Salver-Disma, L. Aymard, L. Dupont, J.M. Tarascon, Effect of mechanical grinding on the lithium intercalation process in graphites and soft carbons, J. Electrochem. Soc. 143 (12) (1996) 3959–3972.
[42] J.R. Dahn, A.K. Sleigh, Shi Hang, B.M. Way, W.J. Weydanz, J.N. Reimers, Q. Zhong, U. von Sacken, Carbons and graphites as substitutes for the lithium anode, in: G. Pistoia (Ed.), Lithium Batteries: New Materials, Developments and Perspectives, Elsevier, Amsterdam, 1994, pp. 2–47.
[43] R. Yazami, From Rome to Como: 20 years of active research on carbon based electrodes for lithium batteries at INP-Grenoble, J. Power Sources 97–98 (2001) 33–38.